Delayed autoignition in Propagating Detonations

Liliana Berson, Rachel Hytovick, Robyn Cideme, Kareem Ahmed
University of Central Florida
Orlando, Florida, United States of America

1 Introduction

Detonations are characterized by a coupled shock flame system propagating at high speed (~2000 m/s). As the detonation propagates the high local Mach number of the shock rapidly raises the pressure and temperature of the reactants leading to rapid reaction. In one-dimensional analysis, the autoignition time and duration of the heat release have been shown to correlate with detonation properties [1], both of which are primarily governed by the activation energy of the mixture and the post-shock. At lower wave speeds, the autoignition time increases rapidly and the heat release rate decreases. However, in realistic, multidimensional detonations, the interaction between the leading shock and reaction zone becomes significantly more complex.

The characteristic feature of propagating detonation waves is the presence of additional shock waves that propagate in the transverse direction of the leading shock. The interactions between these transverse waves give rise to the cellular nature of propagating detonations. This is described as a repeating cycle of transverse wave collision leading to a high speed Mach stem that decelerates into an incident shock before another pair of transverse wave encroach and collide birthing a new cell [2,3]. The underlying cause of the accelerated Mach stem has been extensively studied [2,4,5]. A commonly observed occurrence, particularly in hydrocarbon and near limit detonations, is the presence of large unburnt gas pockets behind the leading shock wave [6,7]. These pockets have been shown to potentially ignite as transverse waves pass over them and in near limit detonations, they are able to support the transverse wave accelerating into a detonation [3,8,9].

In this study the autoignition within the unburnt gas pocket is imaged in a high-aspect ratio facility using simultaneous MHz rate shadowgraph and CH* chemiluminescence. Several oxygen-nitrogen-hydrocarbon mixtures were tested giving a range of detonation properties and behaviors. methane, and acetylene were used as fuels. The triple point collision was shown to behave in 4 distinct ways: an optimized wave where the reaction front is nearly coincident with the shock and no major reaction occurs, a prompt autoignition with an unburned gas pocket reacting simultaneously with the new Mach stem, a delayed autoignition where the unburnt gas pocket ignites after the generation of the Mach stem, and a non-reactive collision where no strong reaction occurs in the unburned gas pocket.

Correspondence to: kareem.ahmed@ucf.edu

2 Experimental Methodology

Experiments were conducted in the National Automated Detonation Facility (NADF), a fully automated modular high-aspect ratio detonation tube. The facility is 3.6m long and separated into several sections. The automation section contains mass flow-controlled source gases that are mixed in crossflow as they enter the driver section of the facility. The automation of the facility allows for substantial data to be collected rapidly with cycle times of 90s-120s. The driver section consists of a pair of Shchelkin spiral predetonators (53 cm long x 19 mm diameter) entering the primary facility followed by a series of perforated plates inducing the deflagration to detonation transition. The channel is initially 25 mm x 100 mm in this section prior to entering a converging nozzle, reducing the channel to 2 mm x 100 mm. A stabilization section (46 cm length) at this internal dimension follows, allowing the wave to relax before entering the test section. Optical windows (85 mm x 50 mm) are placed on either side of the test section allowing optical diagnostics to be used. Triggering is accomplished by a pressure transducer located just ahead of the windows. The channel then suddenly diverges as it enters a dampening section to decouple the detonation. A controlled exhaust port at the end of the facility completes the automation system. Further details of the facility can be found in [10].

The optical diagnostics configuration comprised simultaneous Z-shadowgraph and CH* chemiluminescence. The shadowgraph was recorded at 10MHz with a Shimadzu HPV-X2 camera equipped with a Nikon AF-S NIKKOR 200-500 mm f/5.6E ED VR lens. A 640 nm CAVILUX Smart UHS system with 10ns pulse width was used as the shadowgraph light source. The CH* chemiluminescence was recorded at 5MHz on another Shimadzu HPV-X2 camera equipped with a Nikon AF FX NIKKOR 80-200 mm f/2.8D ED lens with a Vivitar 2x teleconverter. The laser light was expanded onto an 896 mm focal length hyperbolic mirror to collimate it. To reduce space the path was folded using a pair of flat mirrors turning the light 90 degrees. The light was refocused onto a 505 nm dichroic beam splitter to separate the CH* chemiluminescence from the shadowgraph. This allowed the two diagnostic's field of views to be pixel coincidence. The shadowgraph light passes through a 570 nm long pass to eliminate the flame signal and several neutral density filters to optimize the light entering the camera. The chemiluminescence signal turned 90 degrees with another flat mirror before entering the camera. The resolution varied between 154 and 28 μm/pixel to visualize the local detonation structure. Processing the shadowgraph images allowed for the generation of velocity maps. By tracking the shock front in each frame, the local velocity field can be calculated. Details of the method can be found in [10].

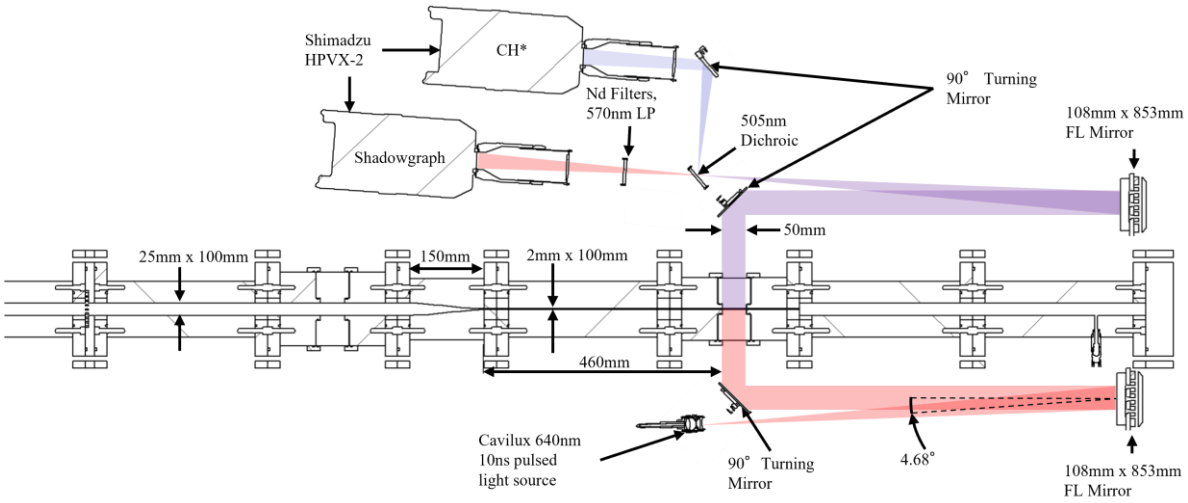

Figure 1: Diagram of the National Automated Detonation Facility and diagnostic setup

The tested conditions and associated detonation parameters are shown in Table 1. These conditions were selected for a representative comparison of the detonation behaviors in regular and irregular mixtures in

near-limit propagation. All parameters were computed in Cantera with the Foundational Fuel Chemistry Model 2.0 [11]. The activation energy was found in the method described in [12]. All conditions were achieved within 1% of the target equivalence ratio and 4% of the target nitrogen dilution. To ensure repeatability each condition was repeated a minimum of 10 times.

Table 1: Test conditions and computed detonation properties

Mixture	D_{CJ}, m/s	E_a/R_uT_{VN}	Δ_i, mm
$0.5CH_4+O_2$	2388	10.3	0.28
$0.5CH_4+O_2+0.43N_2$	2246	10.9	0.58
$0.5CH_4+O_2+N_2$	2120	11.55	1.31
$0.4C_2H_2+O_2+1.5N_2$	2090	4.11	0.05

3 Results

Imaging triple point collisions in the tested conditions showed four types of triple point collisions differing in the size of the unburnt gas pocket, and autoignition location and delay. An image series for each type of collision is shown in Figures 2-5. In the first type (Figure 2), only a small, unburned gas pocket exists behind the incident shock. This unburnt pocket initiates as the encroaching triple points collide with the resulting reaction fully coupling in the generated Mach stem.

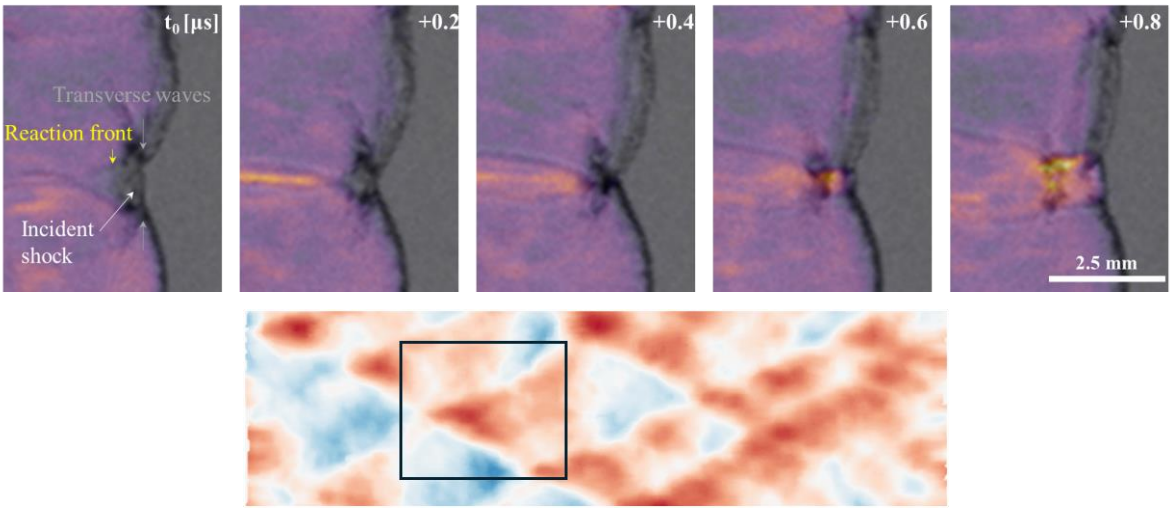

Figure 2: $0.5CH_4+O_2$ Top: Overlaid shadowgraph CH* chemiluminescence, bottom: Velocity map scaled between 1.35 and 0.5 V/D_{CJ} centered at $1V/D_{CJ}$

The second collision type is shown in Figure 3. As the unburnt gas pocket increases in size, the location of the autoignition moves behind the generated Mach stem. The expanding reaction wave pushes the Mach stem strengthening it to an overdriven state and transmits into adjacent boundary layers inducing transverse detonations in the adjacent cell.

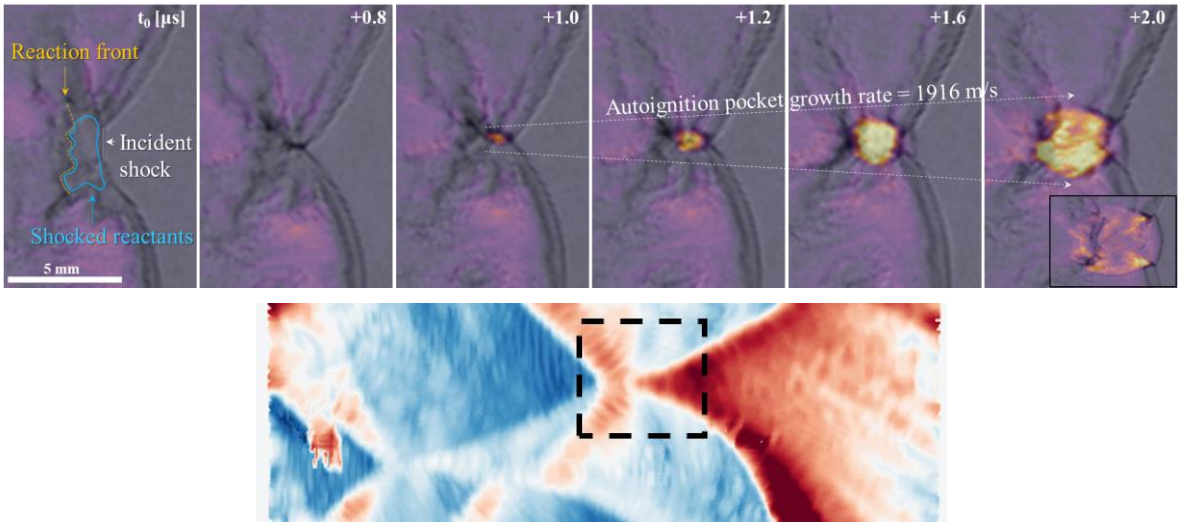

Figure 3: $0.5CH_4+O_2+0.43N_2$ Top: Overlaid shadowgraph CH* chemiluminescence, bottom: Velocity map scaled between 1.35 and 0.5 V/D_{CJ} centered at $1V/D_{CJ}$

In the third type of collision (Figure 4), the unburnt pocket behind the collision ignites ~500ns after the generation of the Mach stem. While the autoignition is present it fails to generate a strong expanding reaction and fails to support the shock front or expanding transverse waves. Additionally, the unburnt gases behind the encroaching transverse waves ignite separately immediately as the waves collide.

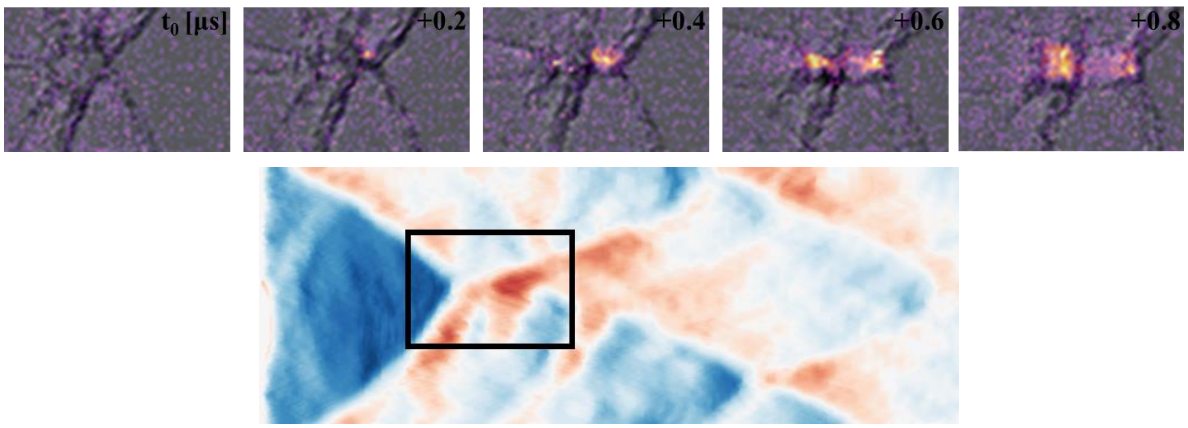

Figure 4: $0.4C_2H_2+O_2+1.5N_2$ Top: Overlaid shadowgraph CH* chemiluminescence, bottom: Velocity map scaled between 1.35 and 0.5 V/D_{CJ} centered at $1V/D_{CJ}$

In the final type of collision observed (Figure 5), the unreacted gas pocket completely fails to ignite and is indicative of a failing portion of the detonation. The jet generated by the counter rotating vortex pair brings hot reactants into the Mach stem allowing the gas in this region to be burned albeit in a diminished manner.

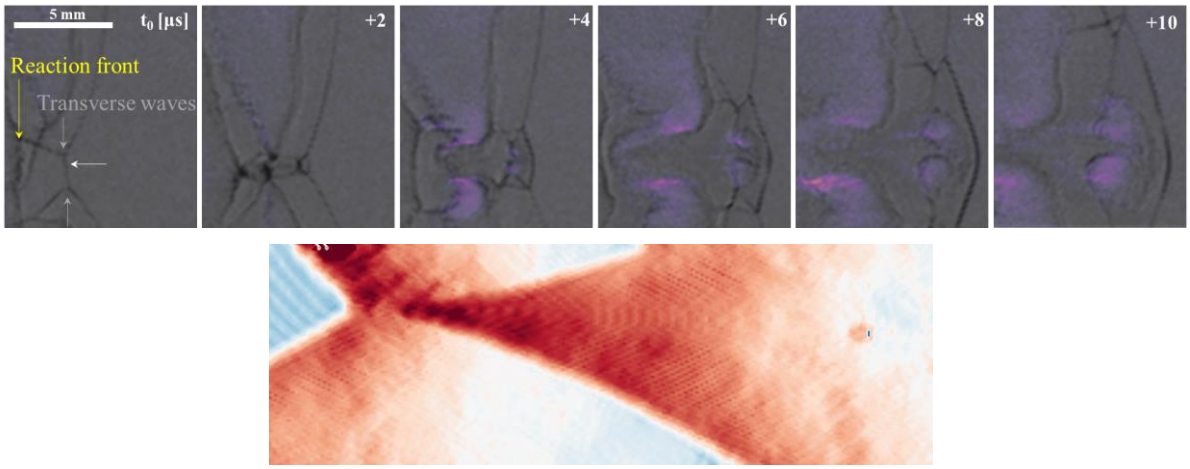

Figure 5: $0.5CH_4+O_2+N_2$ Top: Overlaid shadowgraph CH* chemiluminescence, bottom: Velocity map scaled between 1.05 and 0.5 V/D_{CJ} centered at $1V/D_{CJ}$

4 Discussion and Conclusion

These results indicate that as successful detonations propagate, the unburnt gas pockets in the keystone behind the incident shock autoignite rapidly as the transverse waves collide. This autoignition process is progressively delayed as the detonation limit is approached and the unburnt gas pocket increases in size. In the absolute limit of cellular detonations, the unburnt gas pocket completely fails to ignite, and a large volume of reactants may survive well past the wave.

This behavior can be further interpreted through the effective activation energy and induction length, which vary between mixtures and play a critical role in detonation behavior. In the 2 successful CH_4 collisions, the relatively high activation energy results in greater temperature sensitivity, intensifying the autoignition process. However, in the failed $0.5CH_4+O_2+N_2$ case, this same high activation energy inhibits ignition due to the reduced intensity of both the incident shock and transverse waves.

By contrast, the C_2H_2 mixture, which possesses the lowest induction length and effective activation energy, exhibits ignition not only within the keystone pocket but also behind the upper transverse wave immediately after collision. The smaller induction length leads to a more compact unburnt gas pocket, while the lower activation energy allows the gases to auto ignite with relatively weak shock systems.

These observations suggest that the induction length, driven by the intensity of the leading shock, determines the size of the unburnt gas pocket. Meanwhile, the ability of transverse waves to ignite this pocket depends on their strength relative to the mixture's effective activation energy. Collectively, these mechanisms point to a coupled cellular model in which both the vortex-pair-induced jetting and local autoignition govern the sustenance of the detonation.

5 Acknowledgements

This work is sponsored by the Office of Naval Research (#N00014-22-1-2606, Research Topic Chiefs: Dr. Steve Martens (ONR), Dr. Doug Schwer (NRL), Dr. Chiping Li (AFOSR)), the Air Force Office of Scientific Research (19RT0258/FA9550-19-0322, Program Manager: Dr. Chiping Li), and the National Science Foundation (Award #1914453).

References

[1] H. Ng, Y. Ju, J. Lee, Assessment of detonation hazards in high-pressure hydrogen storage from chemical sensitivity analysis, International Journal of Hydrogen Energy 32 (2007) 93–99. https://doi.org/10.1016/j.ijhydene.2006.03.012.
[2] J.H.S. Lee, The Detonation Phenomenon, Cambridge University Press, 2008.
[3] R.A. Strehlow, A.J. Crooker, The structure of marginal detonation waves, Acta Astronautica 1 (1974) 303–315. https://doi.org/10.1016/0094-5765(74)90100-3.
[4] K. Cheevers, M. Radulescu, Ignition Behind Decaying Shock Waves : Detonation Cells, (2022). http://arxiv.org/abs/2211.05216.
[5] J.E. Shepherd, Detonation in gases, Proceedings of the Combustion Institute 32 I (2009) 83–98. https://doi.org/10.1016/j.proci.2008.08.006.
[6] M.I. Radulesco, G.J. Sharpe, C.K. Law, J.H.S. Lee, The hydrodynamic structure of unstable cellular detonations, Journal of Fluid Mechanics 580 (2007) 31–81. https://doi.org/10.1017/S0022112007005046.
[7] B.M.N. Maxwell, R.R. Bhattacharjee, S.S.M. Lau-Chapdelaine, S.A.E.G. Falle, G.J. Sharpe, M.I. Radulescu, Influence of turbulent fluctuations on detonation propagation, Journal of Fluid Mechanics 818 (2017) 646–696. https://doi.org/10.1017/jfm.2017.145.
[8] J.M. Austin, F. Pintgen, J.E. Shepherd, Reaction zones in highly unstable detonations, Proceedings of the Combustion Institute 30 (2005) 1849–1857. https://doi.org/10.1016/J.PROCI.2004.08.157.
[9] G.L. Schott, Observations of the Structure of Spinning Detonation, The Physics of Fluids 8 (1965) 850–865. https://doi.org/10.1063/1.1761328.
[10] J. Berson, R. Cideme, T.R. Brown, R. Hytovick, K.A. Ahmed, Statistical Variability of Quasi-2D Hydrocarbon Detonations, in: AIAA SCITECH 2024 Forum, 2024: p. 2785.
[11] Y. Zhang, W. Dong, L. Vandewalle, R. Xu, G. Smith, H. Wang, Foundational Fuel Chemistry Model Version 2.0 (FFCM-2), FFCM-2 Website (2023). https://web.stanford.edu/group/haiwanglab/FFCM2.
[12] Q. Xiao, On the geometrical scaling of hydrocarbon detonation dynamics, Combustion and Flame 251 (2023) 112714. https://doi.org/10.1016/j.combustflame.2023.112714.